CELL BIOLOGY

Stress granules sense metabolic stress at the plasma membrane and potentiate recovery by storing active Pkc1

Triana Amen[1] and Daniel Kaganovich[1,2]*

As the physical barrier between the cell and the outside environment, the plasma membrane is well-positioned to be the first responder to stress. The membrane is also highly vulnerable to many types of perturbation, including heat, force, osmotic pressure, lipid shortage, and starvation. To determine whether the structural changes in the plasma membrane of *Saccharomyces cerevisiae* brought about by nutrient stress can be communicated to regulatory networks within the cell, we identified proteins that interact with stress granules (SGs), subcellular structures composed of proteins, and nontranslated RNAs that form when cells are stressed. We found that SG proteins interacted with components of eisosomes, which are subcortical membrane structures with a distinct lipid and protein composition. In response to starvation-triggered phosphorylation of eisosome proteins, eisosomes clustered and recruited SG components, including active Pkc1. The absence of eisosomes impaired SG formation, resulting in delayed recovery from nutrient deprivation. Thus, eisosome clustering is an example of interdomain communication in response to stress and identifies a previously unknown mechanism of SG regulation.

INTRODUCTION

Adaptation to stress requires communication between cellular compartments. Of all of these, the role of the plasma membrane in triggering stress responses is one of the least well understood, despite the fact that it is the location where many stresses are likely to be first detectable (*1*). Much like the cytoplasm, the plasma membrane is partitioned into discrete functional domains, some of which undergo structural changes in response to specific external and intracellular changes (*2*–*5*). In the yeast *Saccharomyces cerevisiae*, one of the domains that has been most extensively studied in the context of stress response is the eisosome compartment (*6*).

Eisosomes are filament-like multiprotein complexes that localize radially throughout the membrane in fungi (*6*–*9*). The two main eisosome components, Pil1 (phosphorylation inhibited by long-chain bases 1) and Lsp1 (long-chain bases stimulate phosphorylation 1), grip the plasma membrane with groove-like Bin/amphiphysin/Rys domains (*10*, *11*) and polymerize into cylindrical structures in vitro (*10*). Eisosome assembly and disassembly are regulated by the phosphorylation of Pil1 and Lsp1 by major regulatory kinases, including Pkh1 (protein kinase B–activating kinase homolog 1) and Pkh2 (Pkh1/2) (*12*, *13*) and kinases that are activated by Pkc1 (the yeast isoform of protein kinase C) (*14*), as well as by other eisosome components (*15*). Although eisosomes are not essential and appear to lack a clearly defined cellular function, they have sparked interest due to their pronounced reorganization during stress and their association with nutrient transporters and protein components of ribonucleoprotein (RNP) granules during starvation, all of which suggest that they may play a protective role in stress responses (*16*–*18*).

Several functions have been proposed for eisosomes, including regulation of cell wall synthesis (*19*), storing a reservoir of plasma membrane in their furrows to withstand sheer stress (*6*, *20*), and regulating RNA decay by recruiting the P body protein Xrn1 (*7*). The strongest available evidence indicates that eisosomes play a protective role during metabolic stress (*16*–*18*). The lateral microdomains that are formed by eisosome assembly protect nutrient transporters that are localized there during nutrient stress due to endocytosis and degradation (*17*, *18*). Eisosome formation is sensitive to nutrient availability and the abundance of cellular sphingolipids and can, in turn, modulate the activity of the nutrient stress mediator target of rapamycin complex 2 (*21*–*24*). This leads to the suggestion that eisosomes may constitute part of a signaling hub for relaying nutrient starvation stress to other compartments.

Here, we investigated the role of eisosome signaling in the nutrient starvation stress response and show that eisosome clustering directly primed the assembly of subcortical stress granules (SGs). SGs respond to a variety of stress signals, propagating them across multiple levels of cellular regulation (*25*–*29*). Because of the presence of nontranslated RNAs, ribosomal subunits, and translation initiation factors in SGs, these structures have been thought to repress translation and perhaps store mRNAs for future use (*30*–*32*). SGs can also recruit and modulate the activities of key signaling proteins, including the nutrient sensor TOR and PKC (*32*–*35*). We found that eisosomes underwent Pkc1-dependent clustering during starvation. Eisosome rearrangement promoted SG assembly, which, in turn, recruited more active Pkc1. The ablation of eisosomes severely hampered SG formation and resulted in a substantial delay of recovery from nutrient deprivation.

RESULTS

SGs associate with eisosomes during starvation

We investigated the subcellular architecture of SGs in the context of glucose starvation (*32*). To uncover transient and peripheral SG interactors, we optimized the proximity-dependent biotinylation (BioID) approach for use in yeast (Fig. 1A and fig. S1, A to C) (*36*). This approach allowed us to visualize SG formation while simultaneously inducing the biotinylation of SG components and nearby proteins in live cells (fig. S1, A to C). We used fusions of two

[1]Department of Experimental Neurodegeneration, University Medical Center Göttingen, Göttingen, Germany. [2]1Base Pharmaceuticals, Boston, MA 02129, USA.
*Corresponding author. Email: daniel.kaganovich@med.uni-goettingen.de

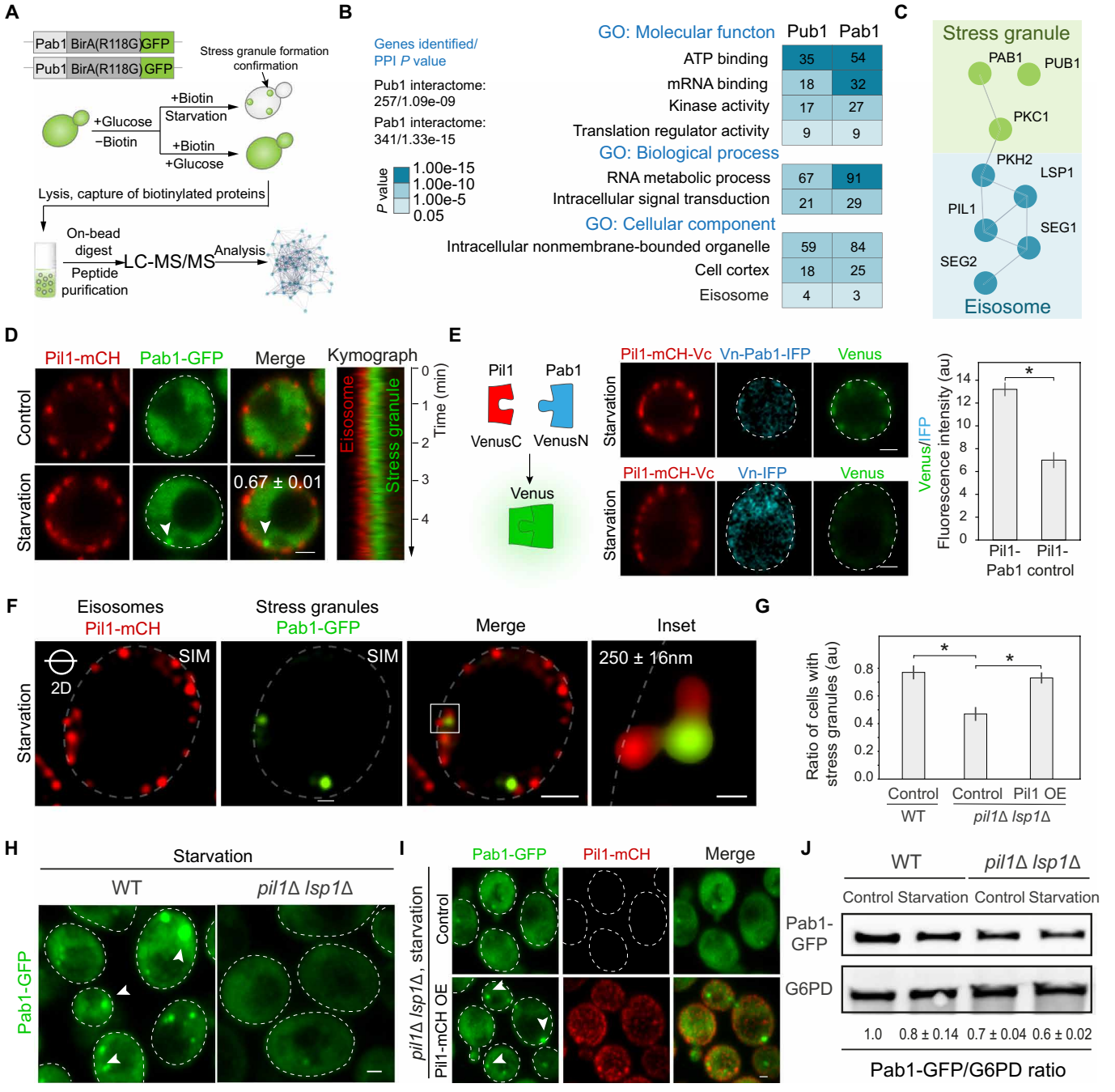

Fig. 1. SGs associate with eisosomes during starvation. (**A**) Strategy for BioID proteomics analysis of yeast proteins adjacent to Pab1 and Pub1 after starvation but not Pab1- or Pub1-adjacent without starvation. LC-MS/MS, liquid chromatography–tandem mass spectrometry. (**B** and **C**) Gene ontology (GO) analysis of SG proteins significantly enriched in Pab1 and Pub1 starvation interactomes hierarchically arranged (B) and eisosome components identified under starvation conditions (C). $n = 3$ biological replicates. ATP, adenosine triphosphate. (**D**) Confocal microscopy of SGs and eisosomes in yeast expressing endogenously tagged Pil1-mCH and Pab1-GFP that were starved for 30 min. Arrowheads indicate SGs. Images and kymograph are representative of four independent experiments. Quantification of the ratio of SGs proximal to eisosomes is noted in the merged images and represent the means ± SEM of 100 cells pooled from all experiments (see also fig. S1I). (**E**) BiFC analysis of Pab1 and Pil1 proximity in cells expressing endogenously tagged Pil1-mCH-VenusC (Vc) and inducible VenusN-Pab1-IFP (Vn) that were starved for 1 hour. Images are representative of three independent experiments. Fold change of fluorescence intensity are means ± SEM of 30 cells per strain pooled from all experiments, $^*P < 0.05$ by Student's t test. (**F**) Live-cell SIM of SG and eisosomes during starvation. Images are representative of four independent experiments. (**G**) Distances between eisosomes and SGs as measured by SIM are indicated as means ± SEM of 30 pairs pooled from all experiments, $^*P < 0.05$ by Student's t test. au, arbitrary units. (**H**) SG formation in wild-type (WT) and *pil1*Δ *lsp1*Δ strains under starvation conditions. Images are representative of three independent experiments. (**I**) SG formation in *pil1*Δ *lsp1*Δ (control) and *pil1*Δ *lsp1*Δ complemented with Pil1-mCH strains under starvation conditions. Images are representative of three independent experiments. (**J**) Western blot for endogenous Pab1 tagged with green fluorescent protein (GFP) in lysates of WT and *pil1*Δ *lsp1*Δ yeast. The numbers below the blot represent combined densitometry results from three independent experiments normalized to WT control, $P = 0.17$ by Kruskal-Wallis test. Scale bars, 1 μm (D, E, F, H, and I) and 200 nm [inset in (F)].

independent SG components (Pub1 and Pab1) to the promiscuous biotin ligase BirAR118G for biotinylating nearby proteins (Fig. 1A and fig. S1E). By subtracting the control interactome from the starvation interactome, we identified a set of candidate SG components and interactors that were either co-assembled with or located proximal to SGs (table S3 and Fig. 1B). We found multiple interactions between SGs and the eisosome complex (Fig. 1, B and C), as well as the kinase Pkh2, which localizes to eisosomes and regulates eisosome assembly (*13*, *14*, *37*, *38*). We observed a strong enrichment of Pkc1 in SGs, which is consistent with the reported localization of PKC to SGs in mammalian cells (*33*). Components of the actin cytoskeleton, actin bodies, also associated with SGs (fig. S1K) (*30*).

We confirmed the interaction between SGs and eisosomes with confocal and structured illumination microscopy (SIM) and bimolecular fluorescence complementation (BiFC) in live cells experiencing starvation stress (Fig. 1, D to F, and fig.S1D; distance between eisosomes and SGs, 250 nm). Eisosomes were consistently associated with SGs, when visualizing the eisosome components Pil1 or Lsp1, during acute starvation or chronic stationary-phase starvation (fig. S1, F and G). Most of the SGs that formed during starvation did so in contact with eisosomes, suggesting that the interaction was not a random phenomenon (Fig. 1, D and F); 67% of the SGs that formed in cells were proximal to eisosomes, as calculated by measuring the overlap in fluorescence intensity peaks (fig. S1H). We also tested whether SGs were associated with eisosomes when they first appeared during starvation (fig. S1, H and I). SGs remained in proximity to eisosomes with little to no movement from the beginning of starvation stress and for 2 hours thereafter (fig. S1, I and J). Eisosomes were also stable during the course of starvation (fig. S3F).

We then examined the nature of the SG-eisosome interaction. BiFC showed that the SG marker, polyA binding-protein 1 (Pab1), was bound to the eisosome core component Pil1 during SG assembly (Fig. 1E and fig. S1L). We asked whether abolishing eisosome complexes by deleting both Pil1 and Lsp1 had an effect on SG formation. Cells without eisosomes had a substantial defect in SG formation (Fig. 1, G and H, and fig. S1M). Complementation of cells in which eisosomes do not form because both *PIL1* and *LSP1* are deleted (*pil1*Δ *lsp1*Δ) with a single copy of *PIL1*-mCherry (mCH) restored SG formation during starvation (Fig. 1, G and I). Cell lacking eisosomes showed a nonsignificant decrease in Pab1 amounts; however, a similar decrease in Pab1 during starvation did not impair SG formation in the wild-type strain and so could not alone explain the SG phenotype observed in the *pil1*Δ *lsp1*Δ strain (Fig. 1J). Together, these data suggested that the eisosome complex plays a direct role in SG formation, and we set out to examine the mechanism of how it may do so.

Eisosome clustering promotes SG formation

We observed that the distance between eisosomes decreased under glucose starvation compared to nonstarved conditions (Fig. 2, A and B), yet the amount of Pil1 in cells remained constant (Fig. 2C). Measuring the average minimal distance between eisosomes on a radial cell section (fig. S2B), we noticed that, upon glucose depletion, Pil1 foci become closer to each other, occasionally forming elongated fibril-like structures (Fig. 2, A and B, and fig. S2, A and B). Total internal reflection–structured illumination (TIRF/SIM) imaging in live cells confirmed the pronounced clustering between eisosomes (Fig. 2A and fig. S2A). Eisosome assembly is known to be regulated by phosphorylation (*13*, *37*, *38*). Mass spectroscopy phosphopeptide analysis showed that Pil1 was phosphorylated at Ser^{163} and Ser^{230} during glucose starvation (Fig. 2D and table S3). We constructed phospho-null S163A and S230A and phospho-mimetic S163D and S230D mutant strains by complementing the *pil1*Δ *lsp1*Δ strain with a single copy of each engineered form of *PIL1* (figs. S2C and S3D). Phospho-null Pil1 overexpression in the eisosome-free background led to impaired eisosome assembly and reduced the formation of SGs during starvation (Fig. 2, E and F). The phospho-mimetic mutant S230D restored the shorter spacing between eisosomes during starvation, as well as the wild-type SG phenotype (Fig. 2, E and F). In addition, we tested the C-terminal disordered region of Pil1, because disordered regions play a role in protein aggregation and clustering, particularly in the case of SGs (*40*, *41*). Complementation of the eisosome-deficient *pil1*Δ *lsp1*Δ strain with Pil1 lacking its C terminus disrupted eisosome structures and failed to nucleate SG assembly during starvation (Fig. 2, E and F). Overall, we found a correlation between SG formation and the average minimal distance between eisosomes (clustering reduces the distance) to be −0.74 (Pearson correlation coefficient). In addition, overexpression of high amounts of wild-type Pil1 resulted in the formation of cytoplasmic fibrils that primed Pab1 assembly (fig. S2D). Reconstituting eisosomes by complementation in *pil1*Δ *lsp1*Δ cells also restored SG formation during starvation (Fig. 2E). Thus, eisosome clustering is a bona fide adaptive response to stress, possibly promoting cellular fitness by priming SG assembly. We also observed that the ability to trigger eisosome clustering during starvation was linked to the replicative age of cells in a dividing yeast population (fig. S2E).

Eisosomes undergo Pkc1-dependent rearrangements during starvation

We next looked at the molecular mechanism of Pil1-dependent eisosome rearrangement. Pil1 is phosphorylated in a Pkc1-dependent manner (*13*), and Pkc1 itself is activated by the kinases Pkh1/2, which are associated with eisosomes (*14*). We were therefore confronted with the intriguing possibility that Pkc1-dependent phosphorylation triggers Pil1 clustering. Pkc1 is an essential signaling protein involved in polarized growth and division, activating downstream kinases of the mitogen-activated protein kinase (MAPK) module, including the MAPK Slt2. To test this feed-forward loop model of Pkc1-mediated Pil1 phosphorylation promoting eisosome reorganization and SG formation, we constructed a yeast strain in which Pkc1 was tagged with an auxin-inducible degradation (AID) and an integrated copy of the OsTIR1 (*42*), allowing us to conditionally deplete cells of Pkc1 by treating them with auxin (fig. S2, F and G, and Fig. 2, G and H). As suggested by the model, Pkc1 depletion abolished eisosome clustering (Fig. 2, G and H). We next asked whether phospho-mimetic mutants of Pil1 could bypass the Pkc1-dependent inhibition of clustering. Overexpression of S163D or S230D mutant forms of Pil1 restored wild-type spacing between eisosomes in response to starvation (fig. S2, I and J). Although it is possible that Pil1 is phosphorylated by downstream kinases of the MAPK module that is activated by Pkc1, and not by Pkc1 itself, we ruled out Slt2 as mediating this modification (fig. S2H). Thus, we argue that Pkc1-dependent phosphorylation of Pil1—and perhaps direct phosphorylation of Pil1 by Pkc1—results in eisosome clustering during starvation.

Active Pkc1 is recruited to SGs

PKC, the mammalian homolog of Pkc1, has been shown to associate with SGs in mammalian cells (*33*). Our BioID analysis showed that Pkc1 is also an SG component in yeast (Fig. 3, A and B, and fig. S3A).

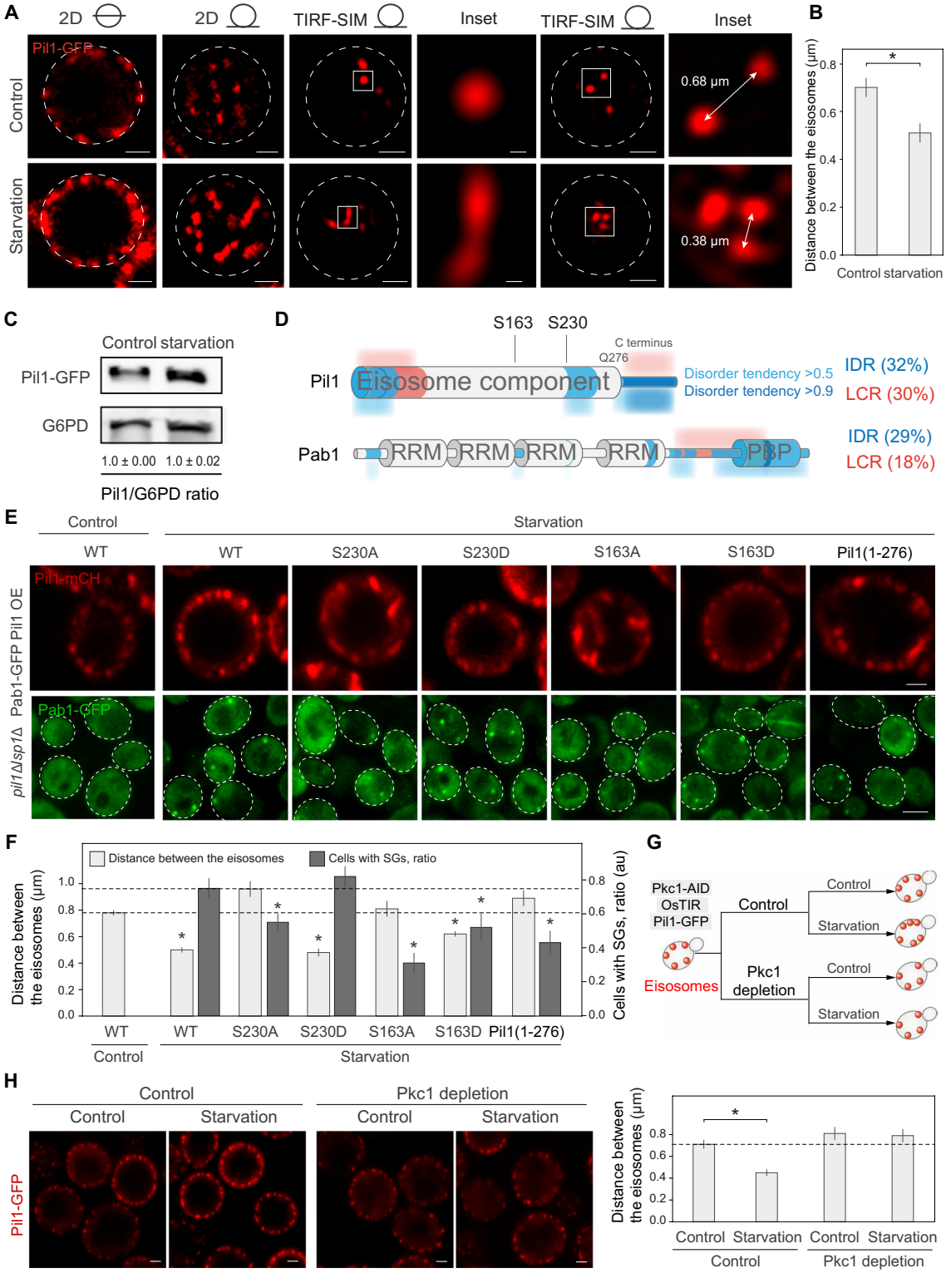

Fig. 2. Pil1 undergoes Pkc1-dependent rearrangements during starvation. (**A**) Confocal and TIRF/SIM microscopy of eisosomes in live yeast expressing endogenously tagged Pil1-GFP and starved for 1 hour. Images are representative of three independent experiments. Imaging plane is indicated above the frames. (**B**) Quantification of the distance between eisosomes on a radial cell section is shown as a mean ± SEM, $*P < 0.05$. Student's *t* test, $n = 100$ cells per condition in three independent experiments. (**C**) Western blot for endogenous GFP-tagged Pil1 in lysates of WT yeast under control and 1-hour starvation conditions. The numbers below the blot represent densitometry combined from three independent experiments, $P = 0.61$ by Mann-Whitney test. (**D**) Schematic of Pil1 and Pab1 showing protein domains, low-complexity regions (LCR), and intrinsically disordered regions (IDR), RNA recognition motif (RRM), and polyadenylate-binding protein domain (PBP). Phosphosites in Pil1 identified during starvation conditions (Ser^{163} and Ser^{230}) are indicated. (**E**) Confocal microscopy in live *pil1*Δ *lsp1*Δ yeast expressing endogenously tagged Pab1-GFP and induced to express mCH-tagged WT, S230A, S230D, S163A, S163D, or truncated (1 to 276) Pil1 before the onset of starvation. Images are representative of three independent experiments. (**F**) Quantification of the ratio of cells in the population with SGs and the distance between the eisosomes. Data represent means ± SEM of 100 cells per strain pooled from all experiments for distance quantification and 1000 cells per strain pooled from all experiments for ratio quantification, $N = 20$. Pearson correlation between SG ratio and the distance between eisosomes = –0.74. Asterisk (*) indicates significant differences in the distance or ratio of cells with SGs comparing to WT, $*P < 0.05$ with one-way analysis of variance (ANOVA). (**G**) Experimental scheme for assessing eisosome formation in yeast expressing endogenously tagged Pkc1-AID, an integrated copy of the auxin receptor OsTIR (*50*), and endogenously tagged Pil1-GFP. Yeast were grown to mid-log phase, and then, Pkc1 depletion was initiated by addition of a synthetic auxin analog before cells were starved and visualized. (**H**) Confocal imaging and quantification of the distance between eisosomes in cells treated as in (G). Data are means ± SEM of 30 cells per group per condition pooled from three independent experiments. Scale bars, 1 μm [A, E (top row), and H), 500 nm [E (bottom row)], and 100 nm (insets in (A)].

Thus, we hypothesized that Pkc1-dependent Pil1 phosphorylation primes SG nucleation by recruiting additional Pkc1. A key prediction of our feed-forward loop model, therefore, is that the Pkc1 recruited to SGs is in an active state. To test whether the active form of Pkc1 was preferentially recruited to SGs, we constructed a strain expressing a copy of Pkc1 R398P, a constitutively active form (Fig. 3A)

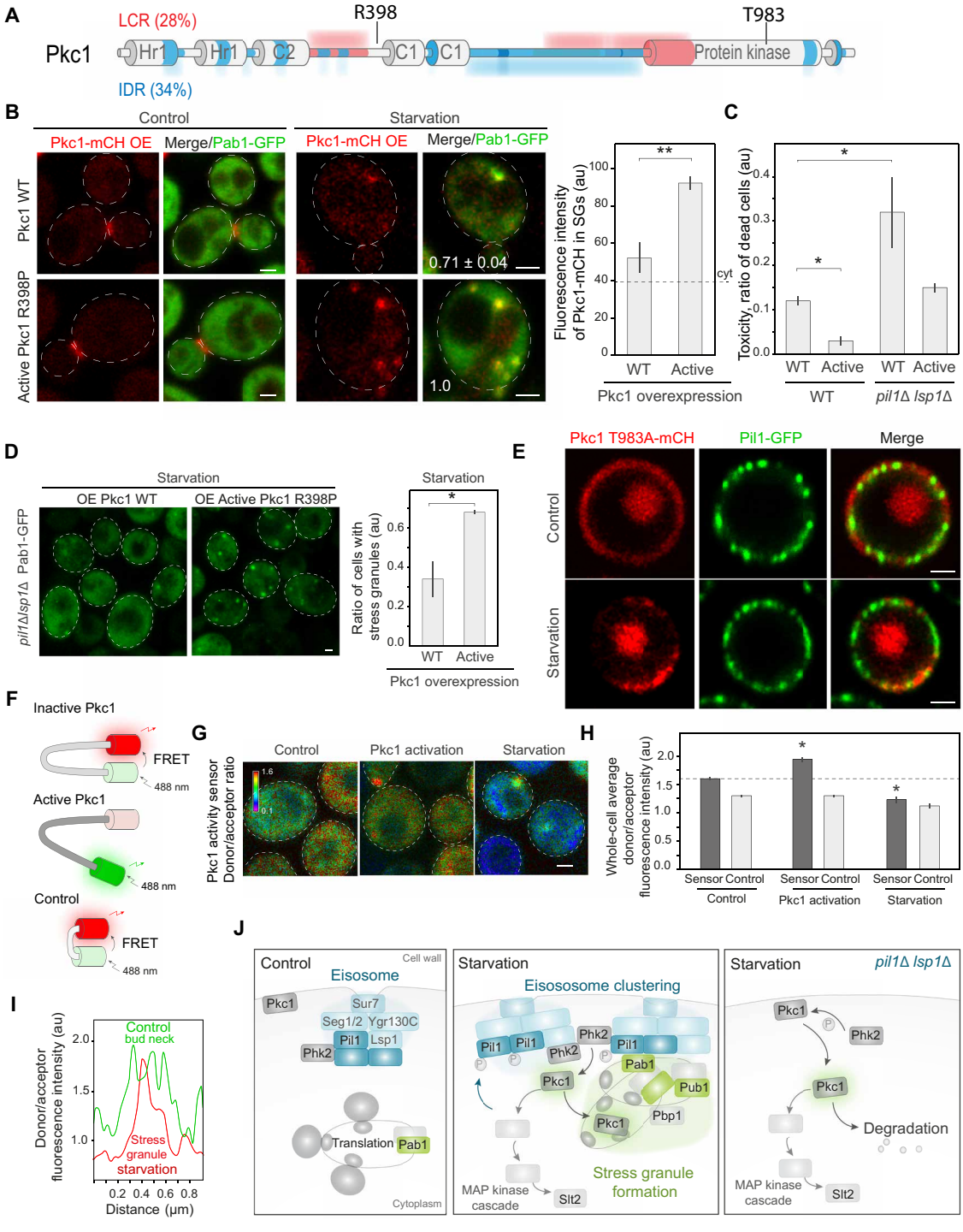

Fig. 3. Pkc1 localizes to SGs and is required for SG formation. (**A**) Schematic of Pkc1 showing protein domains, LCR, and IDRs. The R398P mutation renders Pkc1 constitutively active (*31*). The T983A mutation blocks Pkc1 phosphorylation by Pkh2. (**B**) Live confocal microscopy of yeast expressing endogenously tagged Pab1-GFP and either inducible WT or constitutively active (Pkc1-R398P) Pkc1-mCH grown under control or starvation conditions. Quantified portion of SGs with detectable Pkc1 are noted in the merged images. Fluorescence intensity of Pkc1-mCH in SGs was quantified and presented as means ± SEM from 30 cells per genotype per condition pooled from three independent experiments. $^{**}P < 0.01$. (**C**) Quantified ratios of dead cells in the population of WT and *pil1*Δ *lsp1*Δ yeast overexpressing an integrated copy of Pkc1-mCH or Pkc1-R398P-mCH stained with propidium iodide. Data represent means ± SEM of 100 cells per genotype per condition pooled from three independent experiments. $^{*}P < 0.05$. (**D**) Confocal microscopy of SGs in *pil1*Δ *lsp1*Δ yeast overexpressing Pkc1 or Pkc1-R398P before the starvation and quantification of the ratios of cells in the population with SGs. Data represent means ± SEM of 30 images containing at least 20 cells of each type from three independent experiments. (**E**) Confocal microscopy of yeast expressing endogenously tagged Pil1-GFP and induced to express PKC1(T983A)-mCH 1 hour before starvation. Images are representative of three independent experiments. (**F**) Schematic of FRET sensor for Pkc1 activity and control. Ruby2 (red, acceptor) and Clover (green, donor) are fused to opposite ends of Pkc1. The control is a head-to-tail fusion of Ruby2 and Clover. Activation of Pkc1 is thought to involve a change from a closed to an open conformation (*35*), thus reducing the FRET signal. (**G**) Confocal microscopy showing Pkc1 activity as assessed by FRET in WT yeast grown under control or starvation conditions or in the presence of the Pkc1-activating compound capsofungin. (**H**) Quantification of donor (Clover)/acceptor(Ruby2) fluorescence intensities inside cells during control and starvation conditions. Graphs are representative of 10 independent experiments. Data represent means ± SEM of 30 cells per condition pooled from three independent experiments, $^{*}P < 0.05$, with one-way ANOVA. (**I**) Quantification of FRET activity in (H). (**J**) Model of eisosome rearrangement during starvation. Pkc1-dependent phosphorylation of eisosomes during starvation results in their clustering, which primes formation of SGs that recruit active Pkc1. Scale bars, 1 μm.

(*43*). Overexpression of Pkc1 R398P promoted SG formation, and Pkc1 R398P was also preferentially incorporated into SGs during starvation compared to wild-type Pkc1 (Fig. 3B and fig. S3C), although it was also somewhat toxic. Wild-type Pkc1 exhibited pronounced toxicity in the eisosome-deficient *pil1Δ lsp1Δ* strain (Fig. 3C and fig. S3B).

Overexpression of active Pkc1 restored SG formation during starvation to a wild-type amount in cells lacking eisosomes *(pil1Δ lsp1Δ)*, indicating that Pkc1 activation was sufficient to drive SG formation (Fig. 3D). The links between eisosomes and SGs, therefore, may be Pkh1/2, which can activate Pkc1 and also localize to eisosomes (*14*, *37*). A Pkc1 T983A mutant that is not phosphorylated by Pkh2 (*14*) remained trapped on the membrane and in nuclei (Fig. 3E and fig. S3, G to I) and did not localize to SGs.

Pkc1 stored in SGs rescues cells after starvation

To further confirm that Pkc1 is recruited to SGs in its active form, we constructed a live-cell Pkc1 activity fluorescence resonance energy transfer (FRET) reporter by fusing Ruby2 and Clover to the N and C termini of Pkc1, respectively (Fig. 3F) (*44*). The whole-cell average amounts of Pkc1 activity, as measured by Clover/Ruby2 fluorescence intensity ratio with a single 488-nm excitation, decreased after 1 hour of starvation, indicating an overall decrease in Pkc1 activity (Fig. 3, G and H). The Pkc1 pool localized to SGs, on the other hand, was in an active state, comparable to that of the positive control [Pkc1 activated by caspofungin (*45*)] (Fig. 3I and fig. S3E). This further reinforces the idea that SGs sequester active Pkc1, to reduce its activity elsewhere in the cytoplasm, to store active Pkc1 for a burst of activity following stress resolution, or to create a high local concentration of active enzyme, thereby promoting further eisosome clustering and amplifying the stress signal (Fig. 3J). Pkc1 is necessary for growth and localizes to the bud neck during cell division to promote mitosis (*46*). To understand the functional role of active Pkc1 storage in SGs, we followed the pool of fluorescently tagged Pkc1 (Pkc1-mCH) during long-term starvation and recovery (Fig. 4A). We found that, in recovery after starvation, Pkc1 was able to return to the bud neck after SG clearance in wild-type cells (Fig. 4, A and B). In cells lacking eisosomes, however, Pkc1 failed to relocalize to the bud neck after starvation, likely due to a clear decrease in the amount of tagged protein (Fig. 4B). Hence, without eisosomes and SGs, cells would have to resynthesize Pkc1 after long-term starvation to accumulate the Pkc1 necessary to restart division. As expected, therefore, when we monitored cell growth for 24 hours of recovery from 24 hours in stationary phase, we observed a marked delay in resumption of mitosis in eisosome-deleted cells (Fig. 4, C and D).

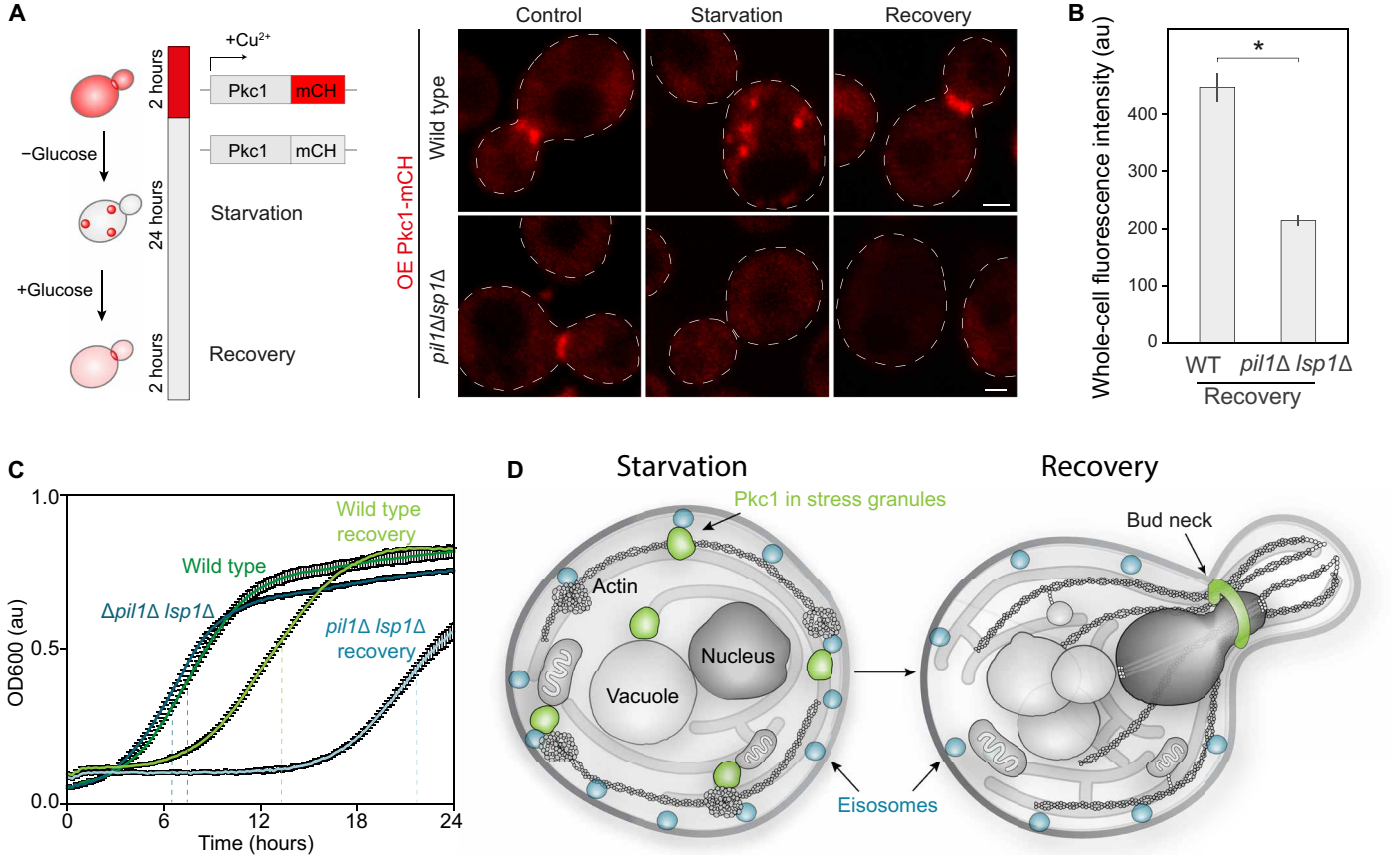

Fig. 4. SGs store Pkc1 and enable rapid recovery from stress. (**A**) Experimental scheme and confocal microscopy of middle-log phase yeast induced to express Pkc1-mCH for 2 hours and then starved for 24 hours before being placed in fresh glucose-containing media for 2 hours. (**B**) Quantification of whole-cell fluorescence intensities from (A). Data represent means ± SEM of 30 cells per genotype per condition pooled from three independent experiments. *$P < 0.05$. (**C**) Growth curves of WT and *pil1Δ lsp1Δ* yeast that were grown under control conditions to middle-log phase or for 24 hours in stationary phase and then diluted in fresh glucose-containing media. Graphs are representative of three independent experiments. Data represent means ± SEM. OD_{600}, optical density at 600 nm. (**D**) Model of WT and *pil1Δ lsp1Δ* recovery after long-term starvation, showing that the absence of SGs results in delayed resumption of division. Scale bars, 1 μm.

DISCUSSION

Efficient adaptation to stress requires integration of several stress response pathways. Here, we showed that, in response to nutrient starvation stress, the structural rearrangement of eisosomes promoted SG formation. One of the key fitness benefits of SG formation in this context appears to be in enabling a faster re-initiation of cell division after stress resolution. We suggest that the eisosome-SG-Pkc1 interaction functions as a feed-forward loop, whereby Pkc1 is responsible for the initial clustering of Pil1, which then primes SG formation by recruiting Pkc1, which, in turn, promotes SG formation (Fig. 3J). Given that Pkc1 is generally in low abundance in the cell and that active Pkc1 is rapidly turned over (*47*, *48*), a feed-forward loop is able to rapidly amplify a local stress signal, resulting in a broad reorganization of cellular resources and saving Pkc1 from degradation (Fig. 3J). This, in turn, allowed cells to restart their growth immediately after SG clearance. In the absence of eisosomes, SGs were less abundant, and without them, Pkc1 was not protected from degradation, which resulted in a delayed recovery after long-term starvation (Fig. 4D).

Our findings resonate with much that is already known about eisosomes, including that Pil1 is phosphorylated in a Pkc1-dependent manner (*13*, *37*) and that phosphorylation induces eisosome rearrangements (*37*). An increase in eisosome density during metabolic stress has also been reported (*17*). The data that we show here add mechanistic detail and extend the functional implications of eisosome dynamics. Our study also presents a previously unknown functionality for SGs and perhaps other RNP granules. Pkc1 promotes RNP granule formation in yeast and mammalian cells (*12*, *33*), and we demonstrated that overexpression of active Pkc1 complemented the SG formation defect in an eisosome-deficient strain. We argue that localization of Pkh2 to eisosomes promotes local Pkc1 activation, which, in turn, induces SG formation, which self-amplifies by recruiting more active Pkc1.

Active Pkc1 is normally degraded by the ubiquitin-proteasome system with rapid kinetics (*48*). This is particularly important in light of the known role of eisosomes in protecting nutrient transporters, including the arginine permease Can1, from degradation (*17*, *18*). An increase in eisosome density during starvation leads to trans-membrane clustering of Can1, which protects this permease from endocytosis and lysosomal degradation (*17*). Our study showed that eisosomes also regulated the subcortical recruitment of active Pkc1 to SGs, where it was protected from turnover and stored until the possibility of growth is restored. In addition, in *Candida albicans*, eisosome complexes help alleviate copper toxicity by maintaining the lipid content of the plasma membrane (*49*). Together, this evidence opens up the possibility of a general protective role for eisosomes during metabolic stress (*16*, *18*).

In addition to illuminating the cellular role of eisosomes in fungi, our model has implications for understanding the biology of SGs and other RNP granules in yeast and in other organisms. By providing a specific context for SG formation within the cellular architecture of yeast, our data raise the question of whether other SG nucleation sites exist in different cellular compartments and whether such nucleation sites might be a universal strategy for differentiating between compartment-specific and cell-wide stress responses.

MATERIALS AND METHODS

Strains and manipulations

We used standard conditions for culturing yeast and bacterial cells (*50*). Yeast strains used in this study are based on BY4741 or W303 (*51*, *52*). We introduced deletions using polymerase chain reaction (PCR)–based deletion strategy (*53*). Gene deletions were verified by PCR using a forward primer upstream of the reading frame and a reverse primer inside the marker reading frame. Yeast transformations were performed using lithium acetate/polyethylene glycol method (*54*) with minor modifications (*55*). The strains used in the study are summarized in table S1. We used copper-inducible expression of *PIL1*. We verified that the levels of copper were not causing additional toxicity to the eisosome-lacking strains as was demonstrated for *C. albicans* (fig. S3D) (*49*).

Plasmid construction

All plasmids were constructed using *Escherichia coli* strain DH5α. Integration was performed using pDK plasmids as backbones (*48*, *55*). Plasmids used in this study are summarized in table S2. Site-directed mutagenesis was verified by sequencing. Plasmids for endogenous tagging were constructed by modifying pKT127 plasmid (*56*).

Protocol for SG induction

Freshly grown yeast culture was diluted and grown in synthetic defined (SD) media to mid-log phase. Cells are pelleted and the media is changed to SD without glucose for the time indicated in the experiment, usually 1 hour. To induce a more prominent SG response, the cells can be transferred to 37°C during starvation (used for SIM and TIRF/SIM imaging). Cells with SG are visualized in the same media, changing the media to glucose will result in fast clearance of inclusions.

Extraction of biotinylated proteins

Yeast strain expressing *PAB1*-BirA(R118G)-GFP or *PUB1*-BirA(R118G)-GFP was grown overnight in YPD (yeast extract, peptone, and dextrose) media, followed by 8 hours in biotin-depleted synthetic defined (SD) media (Formedium). After that, biotin (100 μM) was added to the media, and cells were grown either in glucose-depleted media with subsequent heat stress or SD complete media for 6 hours. SG formation was visualized on the microscope. Cells were harvested and frozen. Lysis and affinity capture were performed according to Roux *et al.* (*36*) with minor modifications. Cells were washed with water and (subsequent steps at 4°C) lysed in the buffer [50 mM tris (pH 7.4), 500 mM NaCl, 0.4% SDS, 5 mM EDTA, 1 mM dithiothreitol (DTT), and 1× ProBlock Gold yeast protease inhibitor cocktail (Gold Biotechnology)] with 425- to 600-μm glass beads (Sigma). After 1 min of vortex, Triton X-100 was added to 2% concentration, and after second round of vortex, equal amount of 50 mM tris (pH 7.4) was added. After third round of vortex and centrifugation, streptavidin-coated magnetic beads (New England Biolabs) were added to the supernatants and incubated overnight at 4°C with agitation. Beads were collected and washed according to Roux *et al.*

Preparing samples for mass spectroscopy

The beads were washed free of detergents by two washes with 25 mM tris-HCl (pH 8.0). Then, the packed beads were resuspended in 100 μl of 8 M urea, 10 mM DTT, and 25 mM tris-HCl (pH 8.0) and incubated for 20 min, followed by addition of iodoacetamide to a concentration of 55 mM and incubation for 20 min in the dark. The urea was diluted by the addition of 6 volumes of 25 mM tris-HCl (pH 8.0), 0.25 μg of trypsin was added (Promega Corp., Madison, WI, USA), and the beads were incubated overnight at 37°C with gentle

agitation. The released peptides were desalted by loading the whole bead supernatant on C18 stage tips (*57*). Two-thirds of the eluted peptide material was used for mass spectroscopy (MS) analysis. For phosphoprotein analysis, the same protocol of reduction, alkylation, and trypsin digestion was followed, but the phospho-peptides were subjected to enrichment by TiO_2 resin (Calbochem ProteoExtract kit) and then desalted on stage tips.

Liquid chromatography–tandem MS analysis

MS analysis was performed using a Q Exactive Plus mass spectrometer (Thermo Fisher Scientific) coupled on-line to a nanoflow ultrahigh-performance liquid chromatography instrument (Ultimate 3000 Dionex, Thermo Fisher Scientific). Eluted peptides were separated over a 150-min gradient run at a flow rate of 0.3 μl/min on a reverse phase 50-cm-long C18 column (75 μm ID, 2 μm, 100 Å, Thermo PepMap RSLC). The survey scans [380 to 2000 mass/charge ratio (*m*/*z*); target value, 3×10^6 charges; maximum ion injection times, 50 ms] were acquired and followed by higher-energy collisional dissociation-based fragmentation (normalized collision energy, 28). A resolution of 70,000 was used for survey scans and up to 15 dynamically chosen most abundant precursor ions were fragmented (isolation window, 1.6 *m*/*z*). The tandem MS (MS/MS) scans were acquired at a resolution of 17,500 (target value, 1×10^5 charges; maximum ion injection times, 120 ms). For samples of TiO_2-enriched phosphopeptides, the MS settings were modified as follows: For survey scans, the maximum ion injection time was 200 ms, and MS/MS scans were acquired at a resolution of 35,000 (target value, 2×10^5 charges; maximum ion injection times, 200 ms).

MS data analysis

Mass spectra data were processed using the MaxQuant computational platform, version 1.5.3.12 (*58*). Peak lists were searched against the *S. cerevisiae* Uniprot FASTA sequence database containing a total of 9591 reviewed entries. The search included cysteine carbamidomethylation as a fixed modification and oxidation of methionine as variable modifications. Peptides with a minimum length of seven amino acids were considered, and the required false discovery rate was set to 1% at the peptide and protein level. Protein identification required at least three unique or razor peptides per protein group. Relative protein quantification in MaxQuant was performed using the label-free quantification (LFQ) algorithm (*59*). LFQ in MaxQuant uses only common peptides for pair-wise ratio determination for each protein and calculates a median ratio to protect against outliers. It then determines all pair-wise protein ratios and requires a minimal number of two peptide ratios for a given protein ratio to be considered valid. For phosphopeptide analysis by MaxQuant, two options were added to the settings: variable modification of phosphorylation at S, T, and Y and dependent peptide search. Identified proteins were analyzed with Cytoscape software (GeneMANIA plugin) (*60*).

Bimolecular fluorescent complementation

We modified BiFC yeast plasmids (*61*) by inserting a mCH-VenusC reading frame in yeast plasmid for endogenous tagging pKT127 (*56*). VenusN fragment was cloned into pDK-HC plasmid for endogenous tagging with subsequent subcloning of *PAB1*-IFP (infrared fluorescent protein) or IFP to extend the open reading frame, resulting in plasmids pDK-HC-VenusN-IFP/pDK-HC-VenusN-*PAB1*-IFP. To detect complementation signal, yeast were grown to mid-log phase in SD media containing 10 μM Cu^{2+}, and then, cells were divided into samples grown under control and starvation conditions. After that, cells were plated and visualized.

Auxin-inducible degradation

We modified pKT127 (*56*) plasmid by introducing AID-HPH (hygromycin B phosphotransferase, hygromycin resistance) fragment for endogenous tagging (*42*). AID-ymRFP pOQR4 plasmid was a gift from M. Lisby. pBabe Blast osTIR1-9Myc was a gift from A. Holland (Addgene plasmid #80073). We integrated OsTIR on pDK-HC plasmid. Pkc1 was endogenously tagged with AID or AID-ymRFP. Yeast cells were grown in SD media to mid-log phase, and $Cu2^+$ was added to a final concentration of 10 μM to induce OsTIR expression. 1-Naphthaleneacetic acid (10 μM; Sigma) or vehicle was added for 3 hours to induce Pkc1 depletion. The cells were then shifted to media with or without glucose for 1 hour to induce SG formation.

Microscopy

For imaging yeast, cells were grown to mid-log phase and seeded on concanavalin A (Sigma)–coated four-well microscope plates (IBIDI). Confocal three-dimensional (3D) images and movies were acquired using a dual point-scanning Nikon A1R-si microscope equipped with a PInano Piezo stage (MCL, Mad City Labs Inc.), using a 60× PlanApo VC (violet corrected) oil objective with a numerical aperture (NA) of 1.40. Movies were acquired in resonant-scanning mode. Image processing was performed using NIS-Elements software. For superresolution SIM, cells were prepared as described above. Images were acquired using a Nikon nSIM microscope with 488- and 561-nm lasers. A 100× oil TIRF objective (NA, 1.49) was used for the imaging. Before imaging, the point-spread function was visualized with 100-nm fluorescence beads to adjust the correction ring of the objective to the coverslip thickness. The final image was reconstructed using NIS-Elements software (Nikon). For superresolution, total internal reflection microscopy cells were prepared as described above. Images were acquired using Nikon nSIM microscope equipped with TIRF module and a 100× Apochromat TIRF oil objective (NA, 1.49) in 2D mode. The final image was reconstructed using NIS-Elements software.

Western blotting

We used the following reagents to detect proteins: anti–green fluorescent protein (GFP) (ab290), anti–glucose-6-phosphatedehydrogenase antibody (Sigma A9521), anti-rabbit immunoglobulin G [horseradish peroxidase (HRP)] (ab6721), streptavidin-Cy3, and streptavidin-HRP (Thermo Fisher Scientific).

Protein sequence analysis

Identification of intrinsically disordered regions (IDRs) and low-complexity regions (LCRs). Prediction of LCRs was performed using SEG software (*62*). Prediction of IDR was performed using IUPred resource (*63*).

Statistics

Three or more independent experiments were performed to obtain the data. *P* values were calculated by two-tailed Student *t* test or one-way analysis of variance (ANOVA) for samples with $n > 10$ following normal distribution. Normal distribution of the data was verified using Shapiro-Wilk test, and the equality of variances was verified by Levene's test. Mann-Whitney or Kruskal-Wallis tests were used for experiments with less than five samples. The sample sizes were not predetermined.

SUPPLEMENTARY MATERIALS

stke.sciencemag.org/cgi/content/full/13/623/eaaz6339/DC1
Fig. S1. SGs associate with eisosomes during starvation.
Fig. S2. Eisosomes undergo Pkc1-dependent clustering during starvation.
Fig. S3. Pkc1 localizes to SGs during starvation.
Table S1. *S. cerevisiae* strains used in this study.
Table S2. Plasmids used in this study.
Table S3. Pab1 and Pub1 interactomes identified by BioID and Pil1 phosphorylation during control and starvation.

View/request a protocol for this paper from *Bio-protocol*.

REFERENCES AND NOTES

1. K. Kono, A. Al-Zain, L. Schroeder, M. Nakanishi, A. E. Ikui, Plasma membrane/cell wall perturbation activates a novel cell cycle checkpoint during G1 in *Saccharomyces cerevisiae*. *Proc. Natl. Acad. Sci. U.S.A.* **113**, 6910–6915 (2016).
2. T. Makushok, P. Alves, S. M. Huisman, A. R. Kijowski, D. Brunner, Sterol-rich membrane domains define fission yeast cell polarity. *Cell* **165**, 1182–1196 (2016).
3. N. E. Ziółkowska, R. Christiano, T. C. Walther, Organized living: Formation mechanisms and functions of plasma membrane domains in yeast. *Trends Cell Biol.* **22**, 151–158 (2012).
4. A. Athanasopoulos, B. André, V. Sophianopoulou, C. Gournas, Fungal plasma membrane domains. *FEMS Microbiol. Rev.* **43**, 642–673 (2019).
5. F. Spira, N. S. Mueller, G. Beck, P. von Olshausen, J. Beig, R. Wedlich-Söldner, Patchwork organization of the yeast plasma membrane into numerous coexisting domains. *Nat. Cell Biol.* **14**, 640–648 (2012).
6. T. C. Walther, J. H. Brickner, P. S. Aguilar, S. Bernales, C. Pantoja, P. Walter, Eisosomes mark static sites of endocytosis. *Nature* **439**, 998–1003 (2006).
7. H. X. Wang, L. M. Douglas, P. Veselá, R. Rachel, J. Malinsky, J. B. Konopka, Eisosomes promote the ability of Sur7 to regulate plasma membrane organization in *Candida albicans*. *Mol. Biol. Cell* **27**, 1663–1675 (2016).
8. R. Kabeche, S. Baldissard, J. Hammond, L. Howard, J. B. Moseley, The filament-forming protein Pil1 assembles linear eisosomes in fission yeast. *Mol. Biol. Cell* **22**, 4059–4067 (2011).
9. I. Vangelatos, K. Roumelioti, C. Gournas, T. Suarez, C. Scazzocchio, V. Sophianopoulou, Eisosome organization in the filamentous ascomycete aspergillus nidulans. *Eukaryot. Cell* **9**, 1441–1454 (2010).
10. L. Karotki, J. T. Huiskonen, C. J. Stefan, N. E. Ziółkowska, R. Roth, M. A. Surma, N. J. Krogan, S. D. Emr, J. Heuser, K. Grünewald, T. C. Walther, Eisosome proteins assemble into a membrane scaffold. *J. Cell Biol.* **195**, 889–902 (2011).
11. A. Olivera-Couto, V. Salzman, M. Mailhos, M. A. Digman, E. Gratton, P. S. Aguilar, Eisosomes are dynamic plasma membrane domains showing pil1-lsp1 heteroligomer binding equilibrium. *Biophys. J.* **108**, 1633–1644 (2015).
12. G. Luo, M. Costanzo, C. Boone, R. C. Dickson, Nutrients and the Pkh1/2 and Pkc1 protein kinases control mRNA decay and P-body assembly in yeast. *J. Biol. Chem.* **286**, 8759–8770 (2011).
13. V. Mascaraque, M. L. Hernáez, M. Jiménez-Sánchez, R. Hansen, C. Gil, H. Martín, V. J. Cid, M. Molina, Phosphoproteomic analysis of protein kinase c signaling in *Saccharomyces cerevisiae* reveals Slt2 mitogen-activated protein kinase (MAPK)-dependent phosphorylation of eisosome core components. *Mol. Cell. Proteomics* **12**, 557–574 (2013).
14. M. Inagaki, T. Schmelzle, K. Yamaguchi, K. Irie, M. N. Hall, K. Matsumoto, PDK1 homologs activate the Pkc1–mitogen-activated protein kinase pathway in yeast. *Mol. Cell. Biol.* **19**, 8344–8352 (1999).
15. K. E. Moreira, S. Schuck, B. Schrul, F. Fröhlich, J. B. Moseley, T. C. Walther, P. Walter, Seg1 controls eisosome assembly and shape. *J. Cell Biol.* **198**, 405–420 (2012).
16. T. Grousl, M. Opekarová, V. Stradalova, J. Hasek, J. Malinsky, Evolutionarily conserved 5′-3′ exoribonuclease Xrn1 accumulates at plasma membrane-associated eisosomes in post-diauxic yeast. *PLOS ONE* **10**, e0122770 (2015).
17. C. Gournas, S. Gkionis, M. Carquin, L. Twyffels, D. Tyteca, B. André, Conformation-dependent partitioning of yeast nutrient transporters into starvation-protective membrane domains. *Proc. Natl. Acad. Sci. U.S.A.* **115**, E3145–E3154 (2018).
18. A. Moharir, L. Gay, D. Appadurai, J. Keener, M. Babst, Eisosomes are metabolically regulated storage compartments for APC-type nutrient transporters. *Mol. Biol. Cell* **29**, 2113–2127 (2018).
19. J. E. Foderaro, L. M. Douglas, J. B. Konopka, MCC/Eisosomes regulate cell wall synthesis and stress responses in fungi. *J. Fungi* **3**, E61 (2017).
20. R. Kabeche, L. Howard, J. B. Moseley, Eisosomes provide membrane reservoirs for rapid expansion of the yeast plasma membrane. *J. Cell Sci.* **128**, 4057–4062 (2015).
21. M. E. Young, T. S. Karpova, B. Brügger, D. M. Moschenross, G. K. Wang, R. Schneiter, F. T. Wieland, J. A. Cooper, The Sur7p family defines novel cortical domains in *Saccharomyces cerevisiae*, affects sphingolipid metabolism, and is involved in sporulation. *Mol. Cell. Biol.* **22**, 927–934 (2002).
22. M. Babst, Eisosomes at the intersection of TORC1 and TORC2 regulation. *Traffic* **20**, 543–551 (2019).
23. J. Zahumensky, J. Malinsky, Role of MCC/Eisosome in fungal lipid homeostasis. *Biomolecules* **9**, E305 (2019).
24. D. Berchtold, M. Piccolis, N. Chiaruttini, I. Riezman, H. Riezman, A. Roux, T. C. Walther, R. Loewith, Plasma membrane stress induces relocalization of Slm proteins and activation of TORC2 to promote sphingolipid synthesis. *Nat. Cell Biol.* **14**, 542–547 (2012).
25. N. Kedersha, P. Ivanov, P. Anderson, Stress granules and cell signaling: More than just a passing phase? *Trends Biochem. Sci.* **38**, 494–506 (2013).
26. N. Kedersha, G. Stoecklin, M. Ayodele, P. Yacono, J. Lykke-Andersen, M. J. Fritzler, D. Scheuner, R. J. Kaufman, D. E. Golan, P. Anderson, Stress granules and processing bodies are dynamically linked sites of mRNP remodeling. *J. Cell Biol.* **169**, 871–884 (2005).
27. A. Khong, T. Matheny, S. Jain, S. F. Mitchell, J. R. Wheeler, R. Parker, The stress granule transcriptome reveals principles of mrna accumulation in stress granules. *Mol. Cell.* **68**, 808–820 e5 (2017).
28. D. Kaganovich, There is an inclusion for that: Material properties of protein granules provide a platform for building diverse cellular functions. *Trends Biochem. Sci.* **42**, 765–776 (2017).
29. T. Amen, D. Kaganovich, Dynamic droplets: The role of cytoplasmic inclusions in stress, function, and disease. *Cell. Mol. Life Sci.* **72**, 401–415 (2015).
30. P. Anderson, N. Kedersha, Stress granules: The Tao of RNA triage. *Trends Biochem. Sci.* **33**, 141–150 (2008).
31. D. S. W. Protter, R. Parker, Principles and properties of stress granules. *Trends Cell Biol.* **26**, 668–679 (2016).
32. J. R. Buchan, J.-H. Yoon, R. Parker, Stress-specific composition, assembly and kinetics of stress granules in *Saccharomyces cerevisiae*. *J. Cell Sci.* **124**, 228–239 (2011).
33. T. Kobayashi, S. Winslow, L. Sunesson, U. Hellman, C. Larsson, PKCα binds G3BP2 and regulates stress granule formation following cellular stress. *PLOS ONE* **7**, e35820 (2012).
34. A. P. Sfakianos, L. E. Mellor, Y. F. Pang, P. Kritsiligkou, H. Needs, H. Abou-Hamdan, L. Déssaubry, G. B. Poulin, M. P. Ashe, A. J. Whitmarsh, The mTOR-S6 kinase pathway promotes stress granule assembly. *Cell Death Differ.* **25**, 1766–1780 (2018).
35. K. Thedieck, B. Holzwarth, M. T. Prentzell, C. Boehlke, K. Kläsener, S. Ruf, A. G. Sonntag, L. Maerz, S. N. Grellscheid, E. Kremmer, R. Nitschke, E. W. Kuehn, J. W. Jonker, A. K. Groen, M. Reth, M. N. Hall, R. Baumeister, Inhibition of mTORC1 by astrin and stress granules prevents apoptosis in cancer cells. *Cell* **154**, 859–874 (2013).
36. K. J. Roux, D. I. Kim, M. Raida, B. Burke, A promiscuous biotin ligase fusion protein identifies proximal and interacting proteins in mammalian cells. *J. Cell Biol.* **196**, 801–810 (2012).
37. T. C. Walther, P. S. Aguilar, F. Fröhlich, F. Chu, K. Moreira, A. L. Burlingame, P. Walter, Pkh-kinases control eisosome assembly and organization. *EMBO J.* **26**, 4946–4955 (2007).
38. G. Luo, A. Gruhler, Y. Liu, O. N. Jensen, R. C. Dickson, The sphingolipid long-chain base-Pkh1/2-Ypk1/2 signaling pathway regulates eisosome assembly and turnover. *J. Biol. Chem.* **283**, 10433–10444 (2008).
39. I. Sagot, B. Pinson, B. Salin, B. Daignan-Fornier, Actin bodies in yeast quiescent cells: An immediately available actin reserve? *Mol. Biol. Cell* **17**, 4645–4655 (2006).
40. S. Kroschwald, S. Maharana, D. Mateju, L. Malinovska, E. Nüske, I. Poser, D. Richter, S. Alberti, Promiscuous interactions and protein disaggregases determine the material state of stress-inducible RNP granules. *eLife* **4**, e06807 (2015).
41. D. Mateju, T. M. Franzmann, A. Patel, A. Kopach, E. E. Boczek, S. Maharana, H. O. Lee, S. Carra, A. A. Hyman, S. Alberti, An aberrant phase transition of stress granules triggered by misfolded protein and prevented by chaperone function. *EMBO J.* **36**, 1669–1687 (2017).
42. M. R. Heider, M. Gu, C. M. Duffy, A. M. Mirza, L. L. Marcotte, A. C. Walls, N. Farrall, Z. Hakhverdyan, M. C. Field, M. P. Rout, A. Frost, M. Munson, Subunit connectivity, assembly determinants and architecture of the yeast exocyst complex. *Nat. Struct. Mol. Biol.* **23**, 59–66 (2015).
43. H. Nonaka, K. Tanaka, H. Hirano, T. Fujiwara, H. Kohno, M. Umikawa, A. Mino, Y. Takai, A downstream target of RHO1 small GTP-binding protein is PKC1, a homolog of protein kinase C, which leads to activation of the MAP kinase cascade in *Saccharomyces cerevisiae*. *EMBO J.* **14**, 5931–5938 (1995).
44. A. J. Lam, F. St-Pierre, Y. Gong, J. D. Marshall, P. J. Cranfill, M. A. Baird, M. R. McKeown, J. Wiedenmann, M. W. Davidson, M. J. Schnitzer, R. Y. Tsien, M. Z. Lin, Improving FRET dynamic range with bright green and red fluorescent proteins. *Nat. Methods* **9**, 1005–1012 (2012).
45. C. Reinoso-Martin, C. Schüller, M. Schuetzer-Muehlbauer, K. Kuchler, The yeast protein kinase C cell integrity pathway mediates tolerance to the antifungal drug caspofungin through activation of Slt2p mitogen-activated protein kinase signaling. *Eukaryot. Cell* **2**, 1200–1210 (2003).
46. V. Denis, M. S. Cyert, Molecular analysis reveals localization of *Saccharomyces cerevisiae* protein kinase C to sites of polarized growth and Pkc1p targeting to the nucleus and mitotic spindle. *Eukaryot. Cell* **4**, 36–45 (2005).

47. B.-S. Kang, O. G. French, J. J. Sando, C. S. Hahn, Activation-dependent degradation of protein kinase Cη. *Oncogene* **19**, 4263–4272 (2000).
48. J. J. Heinisch, R. Rodicio, Protein kinase C in fungi—More than just cell wall integrity. *FEMS Microbiol. Rev.* **42**, fux051 (2018).
49. L. M. Douglas, J. B. Konopka, Plasma membrane architecture protects *Candida albicans* from killing by copper. *PLOS Genet.* **15**, e1007911 (2019).
50. F. Sherman, Getting started with yeast. *Methods Enzymol.* **350**, 3–41 (2002).
51. B. J. Thomas, R. Rothstein, Elevated recombination rates in transcriptionally active DNA. *Cell* **56**, 619–630 (1989).
52. C. B. Brachmann, A. Davies, G. J. Cost, E. Caputo, J. Li, P. Hieter, J. D. Boeke, Designer deletion strains derived from *Saccharomyces cerevisiae* S288C: A useful set of strains and plasmids for PCR-mediated gene disruption and other applications. *Yeast* **14**, 115–132 (1998).
53. A. Baudin, O. Ozier-Kalogeropoulos, A. Denouel, F. Lacroute, C. Cullin, A simple and efficient method for direct gene deletion in *Saccharomyces cerevisiae*. *Nucleic Acids Res.* **21**, 3329–3330 (1993).
54. R. D. Gietz, R. H. Schiestl, A. R. Willems, R. A. Woods, Studies on the transformation of intact yeast cells by the LiAc/SS-DNA/PEG procedure. *Yeast* **11**, 355–360 (1995).
55. T. Amen, D. Kaganovich, Integrative modules for efficient genome engineering in yeast. *Microb. Cell* **4**, 182–190 (2017).
56. M. A. Sheff, K. S. Thorn, Optimized cassettes for fluorescent protein tagging in *Saccharomyces cerevisiae*. *Yeast* **21**, 661–670 (2004).
57. J. Rappsilber, M. Mann, Y. Ishihama, Protocol for micro-purification, enrichment, pre-fractionation and storage of peptides for proteomics using StageTips. *Nat. Protoc.* **2**, 1896–1906 (2007).
58. J. Cox, M. Mann, MaxQuant enables high peptide identification rates, individualized p.p.b.-range mass accuracies and proteome-wide protein quantification. *Nat. Biotechnol.* **26**, 1367–1372 (2008).
59. J. Cox, M. Y. Hein, C. A. Luber, I. Paron, N. Nagaraj, M. Mann, Accurate proteome-wide label-free quantification by delayed normalization and maximal peptide ratio extraction, termed MaxLFQ. *Mol. Cell. Proteomics* **13**, 2513–2526 (2014).
60. J. Montojo, K. Zuberi, H. Rodriguez, F. Kazi, G. Wright, S. L. Donaldson, Q. Morris, G. D. Bader, GeneMANIA Cytoscape plugin: Fast gene function predictions on the desktop. *Bioinformatics* **26**, 2927–2928 (2010).
61. M. K. Sung, W. K. Huh, Bimolecular fluorescence complementation analysis system for in vivo detection of protein–protein interaction in *Saccharomyces cerevisiae*. *Yeast* **24**, 767–775 (2007).
62. J. C. Wootton, Non-globular domains in protein sequences: Automated segmentation using complexity measures. *Comput. Chem.* **18**, 269–285 (1994).
63. Z. Dosztányi, V. Csizmok, P. Tompa, I. Simon, IUPred: Web server for the prediction of intrinsically unstructured regions of proteins based on estimated energy content. *Bioinformatics* **21**, 3433–3434 (2005).
64. Y. Perez-Riverol, A. Csordas, J. Bai, M. Bernal-Llinares, S. Hewapathirana, D. J. Kundu, A. Inuganti, J. Griss, G. Mayer, M. Eisenacher, E. Pérez, J. Uszkoreit, J. Pfeuffer, T. Sachsenberg, Ş. Yilmaz, S. Tiwary, J. Cox, E. Audain, M. Walzer, A. F. Jarnuczak, T. Ternent, A. Brazma, J. A. Vizcaíno, The PRIDE database and related tools and resources in 2019: Improving support for quantification data. *Nucleic Acids Res.* **47**, D442–D450 (2019).

Acknowledgments: We thank W. Breuer for proteomics data acquisition and T. Kneib for statistical consultation. **Funding:** This work was supported by the European Research Council under the European Union's Seventh Framework Programme (FP/2007-2013)/ERC-StG2013 337713 DarkSide starting grant and an EU Joint Programme–Neurodegenerative Disease Research (JPND) 2 grant. T.A. was funded by the Jerusalem Brain Community Doctoral Fellowship for the part of this project. **Author contributions:** All aspects of the work comprising the manuscript were carried out jointly by D.K. and T.A. **Competing interests**: The authors declare that they have no competing interests. **Data and materials availability**: The MS proteomics data have been deposited to the ProteomeXchange (www.ebi.ac.uk/pride) (*64*) with the datasets identifiers PXD016988 and PXD017502. All other data needed to evaluate the conclusions in the paper are present in the paper or the Supplementary Materials.

Submitted 25 September 2019
Accepted 17 February 2020
Published 17 March 2020
10.1126/scisignal.aaz6339

Citation: T. Amen, D. Kaganovich, Stress granules sense metabolic stress at the plasma membrane and potentiate recovery by storing active Pkc1. *Sci. Signal.* **13**, eaaz6339 (2020).

Science Signaling

Stress granules sense metabolic stress at the plasma membrane and potentiate recovery by storing active Pkc1

Triana Amen and Daniel Kaganovich

Sci. Signal. **13** (623), eaaz6339.
DOI: 10.1126/scisignal.aaz6339

Stress granule nucleation at the membrane

In response to stress, eukaryotic cells produce clusters of proteins and RNAs called stress granules (SGs), which sequester mRNAs from the translation machinery until the stress is resolved and may also regulate cellular stress response pathways. Amen and Kaganovich found that, in yeast, SG proteins interacted with components of subcortical structures called eisosomes, which are composed of specific proteins and membrane lipids. Upon starvation, eisosomes clustered and promoted the formation of SGs. Pkc1 (the yeast isoform of protein kinase C) was required for starvation-induced eisosome reorganization and was recruited to SGs in its active form. In the absence of eisosomes, active Pkc1 was not retained in SGs, and recovery from starvation was delayed. These findings identify a mechanism whereby nutrient stress induces structural changes at the plasma membrane that promote the formation of SGs, thus protecting the cell during stress and enabling faster recovery.